Flow Analysis and Optimization of a Hierarchical Plate Heat Exchanger for an Adsorption Heat Pump

Emmerich Tempfli[*1], and Ferdinand P. Schmidt[1]
[1]Fluid Machinery (FSM), Karlsruhe Institute of Technology (KIT)
*Corresponding author: Fachgebiet Strömungsmaschinen, Kaiserstr. 12, 76131 Karlsruhe, Germany, email address: emmerich.tempfli@kit.edu

Abstract: This paper investigates the hydrodynamic performance of a hierarchical parallel channel network for the objective of optimal thermal coupling to heat released in the adsorption processes, as in adsorption heat pumps. More specifically, the uniformity of the fluid flow over the network is improved by optimizing the topology of the manifold channels of the two hierarchical levels. For this purpose a two-step optimization method is applied, utilizing a genetic algorithm coupled with COMSOL Multiphysics. For efficiency reasons, the two hierarchy levels are optimized separately. The hydraulic performance of the optimized topologies is compared with a basic topology.

Keywords: Heat transfer, hierarchical, topology optimization, adsorption heat pump

1. Introduction

Liquid heat transfer is widely-used in systems where high heat transfer rate is required, as in the case of thermally driven heat pumps based on adsorption [1]. By means of compact heat exchangers with plate design (cf. Figure 1) and possibly small fluid channels not only the heat transfer per unit volume but also the solid to liquid heat transfer can be enhanced considerably [2]. An important issue for liquid heat transfer systems is the fluid network design. In this regard, numerous studies investigating the heat transfer performance of various channel networks (such as serpentine [3], parallel [4] and fractal [5]) have been carried out.

Along this line, the aim of this paper is to present a hierarchical channel design which is biomimetic in a sense that the fluid flow is distributed over a 'fractal' manifold to micro porous channels, and subsequently reunited in a 'fractal' manifold again. In the aforementioned channel design, the heat transfer takes predominantly place in the micro porous transitions (see Figure 1). Thus, this is comparable to fractal heat transfer systems evolved in nature with capillary transitions [6].

One of the key issues for the performance of such multi-branching channel networks is the uniformity of the fluid distribution to the sub-channels. In other words, a well distributed flow is necessary to achieve optimal performance in plate heat exchangers. Having this in mind, herein a two-step methodology for the topology optimization of fluid flow in multi-branched channels is presented.

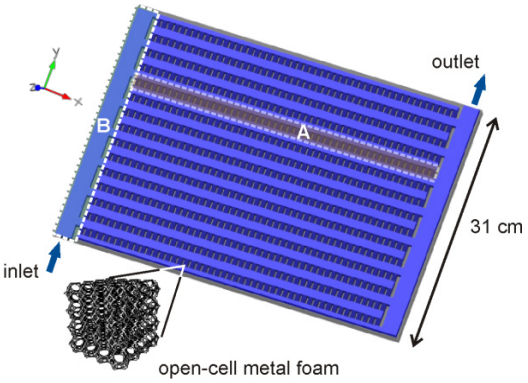

Figure 1 Schematic picture of the hierarchical heat exchanger with the hierarchy levels A and B.

The outline of the paper is as follows. In Section 2, the governing equations of the fluid flow are provided along with the methodology of the topology optimization and the adjustment of the genetic algorithm. The computational specifications are given in Section 3. Furthermore, parametric studies are presented in Section 4. Respectively, in Section 4.1 and Section 4.2, the optimization of the manifold channel of hierarchy level A and B (HLA and HLB) are demonstrated. In Section 5, the concluding remarks based on the key findings are given.

2. Numerical Method

2.1 Governing Equations

In the case at hand, one has a coupling of free media flow with porous media flow. The flow in the open manifold channels is modeled by the Navier-Stokes equation:

$$\rho(\boldsymbol{u}\cdot\nabla)\boldsymbol{u} = -\nabla P + \nabla\cdot\{\mu[\nabla\boldsymbol{u} + (\nabla\boldsymbol{u})^T]\} \quad (1)$$

$$\nabla\boldsymbol{u} = 0, \quad (2)$$

where $\boldsymbol{u}$ is the velocity vector in the open channel, P denotes the pressure, μ denotes the dynamic viscosity and ρ denotes the density of the fluid.

On the other hand, the flow in the micro porous sub-channels is described by the Brinkman equation:

$$\frac{\rho}{\varepsilon}\left((\boldsymbol{u}\cdot\nabla)\frac{\boldsymbol{u}}{\varepsilon}\right) = -\nabla P + \nabla\cdot\{\mu[\nabla\boldsymbol{u} + (\nabla\boldsymbol{u})^T]\} - \frac{\mu}{\kappa}\boldsymbol{u}, \quad (3)$$

$$\nabla\boldsymbol{u} = 0, \quad (4)$$

where κ is the permeability and ε the porosity of the open-cell metal foam.

2.2 Two-step Topology Optimization

As already mentioned, this paper is focused on the use of COMSOL Multiphysics 4.3a with a genetic algorithm (GA) in a custom MATLAB script for topology optimization of the fluid flow problem. The optimization of the two hierarchical levels A and B (cf. Figure 1) is performed separately as can be seen in Figure 3 (a) and Figure 3 (b), respectively.

In general the optimization problem can be formulated in the form

$$\mathrm{Min}_{\boldsymbol{a}}\mathrm{F}(\boldsymbol{a})$$
$$\text{subject to } a_i^{min} \le a_i \le a_i^{max},\ i = 1,\dots,n \quad (5)$$

where F is the objective function and $\boldsymbol{a}$ is a vector of the n design variables a_i.

The optimality of the channel topology is characterized by the uniformity of the flow distribution to the parallel sub-channel arrays. In general, the objective function can be expressed by the variance of the flow distribution in the form:

$$\mathrm{F}(\boldsymbol{a}) = \mathrm{Var}\left[\dot{V}_c(\boldsymbol{a})\right] = \sqrt{\frac{1}{N_c}\sum_{i=1}^{N_c}\left(\dot{V}_{c,i}(\boldsymbol{a}) - \overline{\dot{V}_c(\boldsymbol{a})}\right)^2} \quad (6)$$

where $\dot{V}_{c,i}$ is the flow rate in the i-th sub-channel, $\overline{\dot{V}_c}$ is the mean value of the volume flows and N_c is the sub-channel number.

2.2.1 Optimization Step I

For each of the hierarchy levels A and B, a *two−step* method was chosen in order to improve significantly the performance of the optimization calculations as represented in Figure 2.

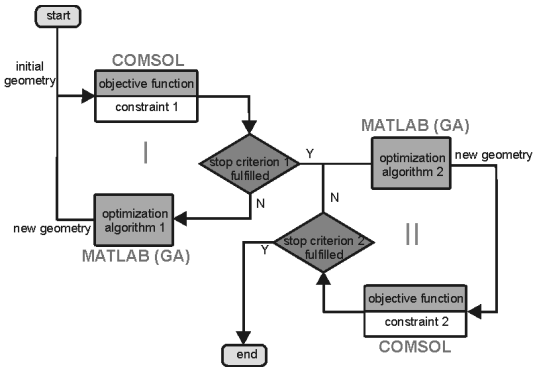

Figure 2 Flow chart of the two-step optimization, with the successive optimization steps I and II, respectively.

In the first optimization step a linear shape function was optimized (OStpI). In order to maintain symmetry and constant channel lengths of the micro porous sub-channels, the following shape function was chosen:

$$\xi_k(\zeta; a) = -\frac{2a}{l_k}\zeta + \left(\frac{w_k^0}{2} + a\right), \quad (7)$$

where ζ denotes the main flow direction and ξ_k the flow direction in the sub-channels. The subscript $k \in \{A, B\}$ denotes the hierarchy level. Here optimization intervals are $a \in \{0, w_A^0/2\}$ and $a \in \{0, w_B^0\}$, for the HLA and HLB, respectively. The optimization algorithm chosen for this step is based on the golden section implemented in MATLAB [7]. This is a robust method with a fast convergence for U-shaped objective functions that are to be expected here.

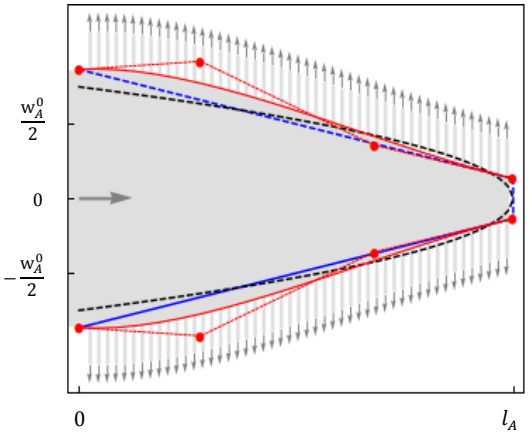

(a)

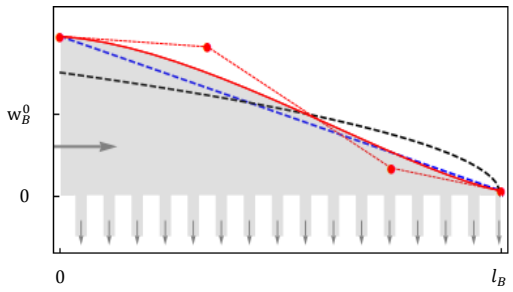

(b)

Figure 3 Topologies of HLA (a) and HLB (b). (Blue dashed) optimized shape Eq. (7); (red solid) optimized shape Eq. (8); (red markers) corresponding control points P_i and (black dashed) shape Eq. (11). (The overall channel shape is indicated by gray shading and the flow by gray arrows.)

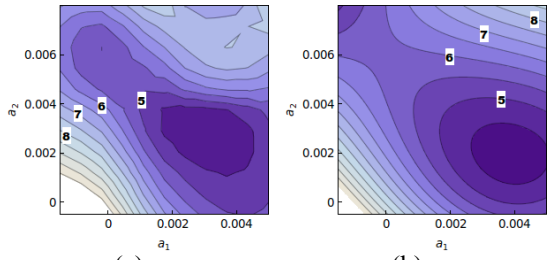

(a) (b)

Figure 4 Contour plot of (a) the calculated data field $\{F_{ij}\}$ and (b) corresponding fitted function $TF(a_1, a_2)$ $[m^3/s]$ given by Eq. (9).

2.2.2. Optimization Step II

In the second optimization step (OStpII) - starting from the result obtained from OStpI - a higher order polynomial is optimized. For OStpII a genetic algorithm (GA) was applied. In order to keep the calculation time in an acceptable range, the polynomial shape function is restricted to a cubic Bézier-curve:

$$\tilde{\xi}_k(\zeta; \boldsymbol{a}) = \sum_{i=0}^{3} \binom{3}{i} \left(\frac{\zeta}{l_k}\right)^i \left(1 - \frac{\zeta}{l_k}\right)^{3-i} P_i(\boldsymbol{a}), \quad (8)$$

with the vector parameter $\boldsymbol{a} = (a_1, a_2)$ and the control points. It should be pointed out that the control points P_1 and P_4 are determined by OStpI.

2.3 Adjusting GA

To make sure that the genetic algorithm of OStpII finds the global minimum, and in order to improve the performance, the parameters of the GA were adjusted by means of a test function adapted to the problem on hand. Since the conventional methods cannot overcome the limitations of flow optimization, stochastic global optimization methods as GA are promising. These are direct search techniques, where the search mechanism is loosely based on biological evolution [8].

The parameter adjustment of the algorithm has been performed using *Genetic Algorithm Toolbox* [9] in MATLAB R2012b. More detailed information about the algorithm and the effect of the parameters can be found in literature [10].

In this study three of the main genetic algorithm parameters, namely the population size (Pop), elite count (Ec), the crossover rate (Xvr) and the mutation rate (Mut) are adjusted with values shown in Table 1 (cf. [11]).

Pop	4	6	8	10
Ec	1	2	3	
Xvr	0.01	0.05	0.1	
Mut	0.6	0.7	0.8	0.9

Table 1 Parameters for adjusting the GA.

δ	Pop	Ec	Xvr	Mut
0	6	2	0.7	0.0053
0.3	6	2	0.65	0.0045

Table 2 Best parameters for GA.

As no general conclusion concerning the optimum parameterization of operators is available, the parameters of the GA were adjusted with a test function (TF). Such a TF is

an analytical function with the features of the problem at hand (cf. Figure 4), but can be analyzed very quickly compared to the actual optimization problem F [Eq. (6)].

The TF is a least-square fit to a calculated data field $\{F_{i,j}\} = \left\{\left(a_1^{(i)}, a_2^{(j)}, F\left(a_1^{(i)}, a_2^{(j)}\right)\right)\right\}$ $(i,j \in \{1,2,\ldots,5\})$. The resulting polynomial is of the form:

$$\mathrm{TF}(a_1,a_2) = \alpha_{01}\cdot\sin(\alpha_{11}\cdot a_1+\alpha_{12})\cdot \sin(\alpha_{21}\cdot a_1+\alpha_{22})+\alpha_{02}[\cos(\alpha_{03})\cdot a_1 - \sin(\alpha_{03})\cdot a_2+\alpha_{04}+\delta\cdot \mathrm{Mod}(a_1,a_2)]. \quad (9)$$

This is a smooth and convex function (cf. Figure 4), where an additional sinusoidal disturbance (Mod) was added for creating local minima.

In Table 2 the best parameter settings are summarized. The application of a disturbance δ has no relevant effect. The population size (Pop) affects both the overall performance and the efficiency of GAs, especially the computational cost. Therefore lowest Pop with no significant effect on the optimization result was chosen for further calculations.

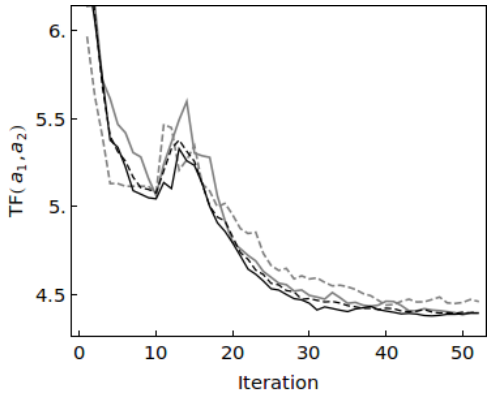

Figure 5 Averaged TF for different populations Pop=4 (gray dashed); Pop=6 (gray solid); Pop=8 (black dashed) and Pop=10 (black solid).

The convergence does not significantly deteriorate down to Pop=6. Furthermore, a convergence is obtained after 40 Iterations (cf. Figure 5). This setting was used for the two-step optimization calculations.

2.4 Basic Topology

If one considers a perfect uniform flow distribution over the sub-channels, the volume flow along the manifold channel decreases linearly with the axial position $\dot{V}(\xi) = (1-\xi/l_k)$. Such a uniform distribution implies a constant drop in the pressure across each sub-channel. This is assured if the pressure along the supply and respectively in the return channels drops linearly with the same gradient. A nonlinearity of the pressure drop can be compensated by a nonlinear manifold topology. For the simple case of a laminar, fully developed flow and a constant friction factor, one obtains a manifold topology (BS) of the form [12]:

$$w_k = \tilde{w}_k^0 \cdot \left(1-\frac{\xi}{l_k}\right)^{\frac{1}{2}}. \quad (10)$$

This channel topology ensures a constant pressure drop across all sub-channels and consequently a uniform flow distribution. In the present study $\tilde{w}_k^0 = 3/2 w_k^0$ in order to keep the volume fractions of the BS channels equal to the optimized ones.

3. Computational Model and Performance

The simulated entity of HLA was taken based on symmetry considerations (cf. Figure 1 and 6). Laminar flow conditions were set at the inlet and no viscous stress was assumed at the outlet. The domain was meshed with approximately 2.5×10^5 tetrahedral elements for mesh independent solutions.

For optimizing HLB (cf. Figure 1), HLA was reduced to an isotropic porous zone connecting the two manifolds as can be seen in Figure 10.

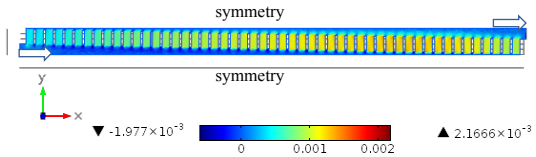

Figure 6 HLA: Velocity field $v_y\,[m/s]$ for $\dot{V}_{tot} = 1\,l/min$ and $\varepsilon = 0.825$. Plane taken at $z = h/2$.

The effective porosity was adjusted to give the same pressure drop as the real structure of HLA (where the real permeability in the micro porous channels was set to $\kappa = 7\cdot 10^{-10}\,m^2$). Here the tetrahedral mesh consists of approximately 5×10^5 elements. The boundary conditions were set accordingly to HLA.

Regarding the computational performance for HLA, convergence of the two-steps optimization is obtained after approx. $t_A \sim 3 \times 10^5\ sec$, and for HLB the computational time is approx. $t_B \sim 4 \times 10^5\ sec$. The computations were performed on a workstation with a quad-core processor (3.33 GHz) and 64 GB of RAM.

4. Parametric Study

The dimensions of the channel network - presented here - were set according to the requirements of an adsorption heat pump. All hierarchy levels possess the same height $h = 3.7\ mm$. The 51 micro porous channels are distributed equidistantly along the manifold of HLA, and have the length $l_{mic} = 5\ mm$ and the width $w_{mic} = 3\ mm$. The dimensions of the initial rectangular manifold of HLA have the dimensions $w_A^0 = 5\ mm$ and $l_A = 19.8\ cm$. From the manifold of HRB 16 sub-channels are branching off. The manifold of HLB possesses the initial dimensions $w_B^0 = 1\ cm$ and $l_B = 31\ cm$. It should be noted that the hierarchical network is symmetric, that is in- and outflow side can be interchanged. Moreover, the topology optimization keeps the volume fractions of the hierarchy levels approximately constant.

$\begin{pmatrix} \varepsilon\ [\%] \\ \kappa\ [10^{-10}\ m^2] \end{pmatrix}$	$\begin{pmatrix} 66.7 \\ 3.88 \end{pmatrix}$	$\begin{pmatrix} 82.5 \\ 23.0 \end{pmatrix}$	$\begin{pmatrix} 87.4 \\ 36.7 \end{pmatrix}$
$\dot{V}_{tot}\ [l/min]$	0.5	1.0	2.0

Table 3 Parameter list for HLA optimization.

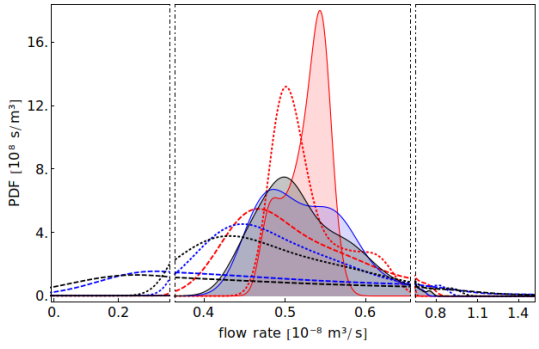

Figure 7 HLA: Smoothed PDF $[s/m^3]$ of the sub-channel flow rates with $\dot{V}_{tot} = 0.5\ l/min$ of different topologies: initial rectangular (dashed); BS Eq. (10) (dotted) and OStpII Eq. (8) (solid) with $\varepsilon = 0.667$ (red); $\varepsilon = 0.825$ (blue) and $\varepsilon = 0.867$ (black), respectively.

4.1 Results for HLA

In the parametrical study of HLA the compressed open-cell foam specifications presented by Boomsma [13] were used. The overall flow rates $\dot{V}_{tot}$ at the inlet of the manifold of HLB were set to values typically occuring in adsorption heat pumps. The calculated data field is summarized in Table 3 in Section 2.3.

One result of the two-step optimization for HLA is shown in Figure 6. The optimized manifold shapes are highly tapered. Due to the unfavorable length-width ratio of the manifold, no perfect uniform distribution of the flow is possible. The quality of uniformity can be best analyzed by means of a probability density function (PDF) of the sub-channel flow rates. A direct comparison of the smoothed PDFs for an overall flow rate $\dot{V}_{tot} = 0.5\ l/min$ is shown in Figure 7.

The perfect uniform distribution would be a Dirac-distribution. Apparently the initial rectangular shape shows a very poor performance compared to the basic topology (BS) and the two-step optimization result (OStpII). In the case of rectangular topology the flow is undamped until it impinges on the channels end, where the flow is redirected into the sub-channels. That is displayed in the PDF representation by a high percentage of low flow rates and a smaller percentage of relatively high flow rates that are located close to the stagnation point of the main flow. Therefore a tapered topology is essential. It could be shown that, the simplified assumptions on which BS is based,

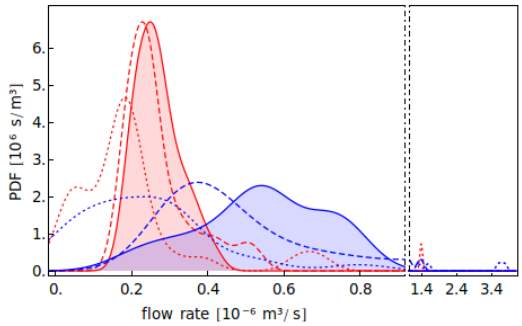

Figure 8 HLB: Smoothed PDF $[s/m^3]$ of the sub-channel flow rates with $\dot{V}_{tot} = 0.5\ l/min$ (red) and $\dot{V}_{tot} = 1\ l/min$ (blue) of different topologies: initial rectangular (dotted); BS Eq. (10) (dashed) and OStpII Eq. (8) (solid).

are no more applicable. A comprehensive direct comparison of the parametrical study is given in Figure 9. Here the objective functions F [cf. Eq. (6)] are shown. Apparently the tapering of the manifolds becomes more important towards higher flow rates $\dot{V}_{tot}$ and higher permeability values κ. In all cases, the two-step optimization gives a significant improvement compared to the BS topology.

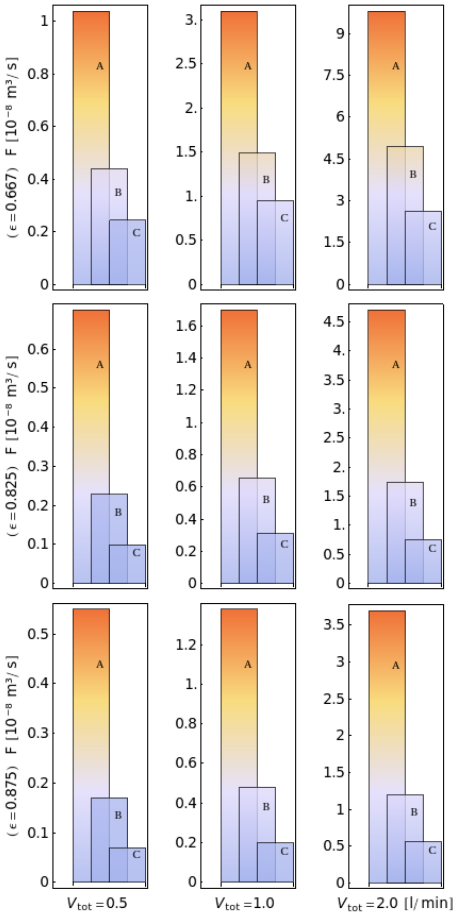

Figure 9 Objective function F $[m^3/s]$ for the calculated parameter field of HLA: Initial rectangular topology (A); BS Eq. (10) (B) and OSptII Eq. (8) (C).

4.2 Results for HLB

The parametric study was restricted to constant effective isotropic permeability κ_{eff} in the porous zone connecting the two manifolds of HLB (cf. Figure 10). This is a simplification of the HLA in order to effect a pressure drop comparable to the setting of a medium porosity open-cell foam ($\varepsilon = 0.7$) in the sub-channels of HLA.

The calculations were again conducted for the overall flow rates $\dot{V}_{tot}$ given in Table 3. The poor performance of the initial rectangular topology is even more striking compared to HLA, for the reason discussed in Section 4.1. The volume flow is mainly going through the last sub-channels (in main inflow direction) as can be seen in the high flow rate parts in Figure 8. For low overall flow rates ($\dot{V}_{tot} = 0.5\ l/min$) the optimized topology and the BS become comparable as is also reflected in the PDFs Figure 8. But for increasing flow rate (cf. $\dot{V}_{tot} = 1\ l/min$ in Figure 8) the flow conditions cannot be approximated in the way done for BS Eq. (10). This is reflected in the significant difference of the PDFs, respectively. The optimal topologies for higher $\dot{V}_{tot}$ become comparable to that of HLA with again a significant improvement compared to the BS in all studied cases (see Figure 11).

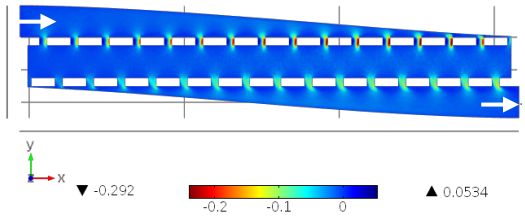

Figure 10 HLB: Velocity field v_y $[m/s]$ for $\dot{V}_{tot} = 1\ l/min$. Plane taken at $z = h/2$.

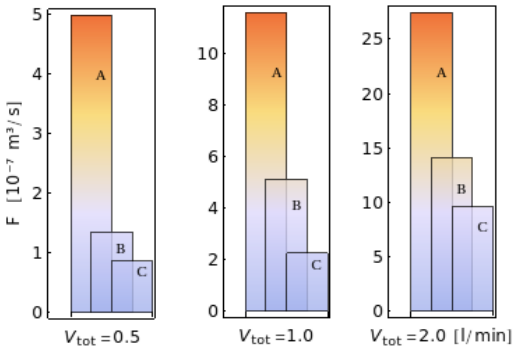

Figure 11 Objective function F $[m^3/s]$ of HLB: Initial rectangular topology (A); BS Eq. (10) (B) and OSptII Eq. (8) (C).

5. Conclusion

An efficient two-step optimization method for topology optimization with COMSOL Multiphysics linked to a standard genetic algorithm (GA) was presented. In line with this, the adjustment of the GA for a hierarchical flow network problem was described. The performance was tested on a hierarchical flow network which was adapted to the application in adsorption heat pumps. Parametric studies were performed for the two hierarchical levels separately. Moreover, the resulting topologies were compared to a basic 'optimal' topology (cf. Section 2.4). The better performance of the two-step optimization could be stated in all calculated cases. Last but not at least, the necessity of 3D simulations for appropriately optimized topologies was shown.

6. References

[1] H. Demir, M. Mobedi, and S. Ülkü, A review on adsorption heat pump: Problems and solutions, *Renewable and Sustainable Energy Reviews*, **12**, pp. 2318-2403 (2008).

[2] D. Tuckerman, and R.F.W. Pease, High-performance heat sinking for VLSI, *Electronic Device Letters, IEEE*, **2**, pp. 126-129 (1981).

[3] J.-Y. San, and K.-L. Pai, Performance of a serpentine heat exchanger: part II - Second-law efficiency, *Applied Thermal Engineering*, **29**, pp. 3088-3093 (2009).

[4] X.L. Xie, Z.J. Liu, Y.L. He, and W.Q. Tao, Numerical study of laminar heat transfer and pressure drop characteristics in a water-cooled minichannel heat sink, *Applied Thermal Engineering*, **29**, pp. 64-74 (2009).

[5] D. Pence, The simplicity of fractal-like flow networks for effective heat and mass transport, *Experimental Thermal and Fluid Science*, **34**, pp. 474-486 (2010).

[6] M.M. Chen, and K.R. Holmes, Microvascular contributions in tissue heat transfer, *Annals of the New York Academy of Science*, **335**, pp. 137-150 (1980).

[7] R. Brent, *Algorithms for Minimization without Derivatives*, Dover Publications, Mineola, NY (2002).

[8] L. Gosselin, M. Tye-Gingras, and F. Mathieu-Potvin, Review of utilization of genetic algorithms in heat transfer problems, *International Journal of Heat Transfer*, **52**, pp. 2169-2188 (2009).

[9] A. Popov, *Genetic Algorithm for optimization-programs for MATLAB*, User Manual, Version 1.0, Hamburg (2005).

[10] A.J. Chipperfield, R. Fleming, H. Pohlheim and C.M. Fonseca, *Genetic Algorithm Toolbox for Use with MATLAB*, User's Guide, Version 1.2, University of Sheffield, Sheffield, UK (1994).

[11] A.E. Eiben, R. Hinterding, and Z. Michalewicz, Parameter control in evolutionary algorithms, *Evolutionary Computation, IEEE Transactions on*, **3**, pp. 124-141 (1999).

[12] W. Esher, B. Michel, and D. Poulikakos, Efficiency for optimized bifurcating tree-like and parallel microchannel networks in the cooling of electronics, *International Journal of Heat and Mass Transfer*, **52**, pp. 1421-1430 (2009).

[13] K. Boomsma, and D. Poulikakos, Metal foams as compact high performance heat exchangers, *Mechanics of Materials*, **35**, pp. 1161-1176 (2003).

7. Acknowledgements

This work was supported by funding of DBU (Deutsche Bundesstiftung Umwelt).